International Journal of Science and Research (IJSR)
ISSN: 2319-7064
Impact Factor 2024: 7.101

Influence of MoS_2 Decoration on ZnO Nanorods for Enhanced Photocatalytic Applications

Priyavrat[1, α], Ariba Khan[2, α], Anil Kumar Singh[1*], Jamilur. R. Ansari[2*]

[1]University Department of Physics, Veer Kunwar Singh University, Ara, Bihar – 802301, India
Email: *tiwari. priyavrat[at]gmail.com,*

[2]Department of Applied Science, Laxmi Devi Institute of Engineering and Technology, Alwar-301028, (Rajasthan), India.
Email: *ariba13khan[at]gamil. com,*
[α] These Authors contribute equally

*Corresponding Authors: Dr. Jamilur R. Ansari, Email: *drjransari[at]gmail.com*
Dr Anil Kumar Singh, Email: *anilkrvksu. ara[at]gmail.com*

Abstract: ***Molybdenum disulfide (MoS_2) and its related two-dimensional materials have emerged as significant subjects of investigation due to their exceptional characteristics, including high catalytic efficiency, remarkable photoluminescent properties for bio-imaging, and superior electronic performance. Recent advancements suggest that doping MoS_2 with metal oxides, particularly zinc oxide (ZnO), can further elevate these properties. In this study, we synthesized pristine MoS_2 nanosheets alongside ZnO-MoS_2 hybrid structures utilizing a solvothermal synthesis method. ZnO is noted for its advantageous properties, such as a wide bandgap, lower energy barriers for charge carrier mobility, and strong thermal and chemical stability. The structural morphology and dimensional characteristics of the ZnO-MoS_2 hybrids were thoroughly analyzed through high-resolution transmission electron microscopy (HRTEM), X-ray photoelectron spectroscopy (XPS), ultraviolet-visible (UV-Vis) spectroscopy, and Fourier-transform infrared spectroscopy (FTIR). The results demonstrated a uniform distribution of ZnO nanorods coated with MoS_2 nanosheets. In photocatalytic assessments, the ZnO and ZnO-MoS_2 hybrids achieved degradation efficiencies of 41% and 81%, respectively, for a 5 μM methylene blue (MB) solution. The corresponding rate constants for the degradation processes were computed as 29.1×10^{-3} min^{-1} for ZnO and 74.1×10^{-3} min^{-1} for ZnO-MoS_2 over a 45-minute exposure to UV light. Quantitative analysis of the absorption spectra was conducted using a UV spectrophotometer, reinforcing the potential application of these hybrid materials in the photocatalytic degradation of environmental contaminants.***

Keywords: MoS_2 nanosheets, ZnO nanorods, methylene blue, photocatalysis, XPS

1. Introduction

This work focuses on the synthesis of high-purity MoS_2, ZnO, and ZnO-MoS_2 hybrid structure using both ultrasonication and sol-gel methods. The resulting MoS_2, ZnO, and ZnO-MoS_2 hybrid structures were meticulously examined for their photocatalytic properties, particularly in the degradation of Methylene Blue dye. A significant highlight of this research is the successful creation of novel ZnO-MoS_2 hybrid structures synthesized through the solvothermal process. The photocatalytic performance of this innovative catalyst was rigorously tested for the breakdown of organic dyes, specifically Methylene Blue (MB), under ultraviolet light exposure. The samples were subjected to irradiation for up to 45 minutes using direct solar energy, showcasing the potential of this approach in developing photocatalysts aimed at addressing water pollution challenges [1–3]. A diverse array of semiconductor materials has been thoroughly explored for their potential in energy production and environmental remediation [4–6]. Among these, zinc oxide (ZnO) has emerged as a particularly compelling candidate due to its remarkable properties. With a large band gap of approximately 3.37 eV, high exciton binding energy, nontoxicity, and excellent electron mobility, coupled with its abundance in nature, ZnO has garnered extensive attention in recent research endeavors [7–9]. However, it is important to note that ZnO's ability to absorb the solar spectrum is limited; it can only capture about 5% of the total solar energy in the ultraviolet (UV) region due to its substantial band gap energy.

High-resolution transmission electron microscopy (HRTEM) analyses have illuminated the intricate morphology and dimensions of the synthesized MoS_2, ZnO, and ZnO-MoS_2 hybrid structures, revealing that they are composed of nanorods expertly coated with MoS_2. Furthermore, the results of photocatalytic degradation experiments demonstrate that the as-synthesized ZnO and ZnO-MoS_2 hybrid structures exhibit impressive degradation efficiencies of 41% and 81%, respectively, when treating a 5 μM methylene blue (MB) solution. ZnO, recognized as an n-type semiconductor due to its wide band gap and ease of synthesis, stands out for its economical fabrication methods and exceptional performance in the UV spectrum, reinforcing its status as a highly effective photocatalytic agent [10–12].

This study details the successful fabrication of ZnO-MoS_2 hybrid structures as a photocatalyst, prepared through a solvothermal synthesis approach [13]. The photocatalytic activity for the degradation of methylene blue (MB) under UV irradiation was evaluated, with exposure times extending to 45 minutes. The maximum absorbance for MB was detected at 660 nm, and the degradation kinetics were characterized by first-order behavior [14, 15]. The creation of ZnO-MoS_2 hybrid structures as heterojunctions remarkably boosted photocatalytic performance by effectively promoting the separation of charge carriers, which in turn led to enhanced efficiency. A comprehensive exploration of the photocatalytic mechanism illuminated the essential roles played by photogenerated holes and hydroxyl

radicals in the degradation process, highlighting their critical contributions to the overall reaction dynamics [16–18].

This research presents an innovative strategy for the development of bifunctional photocatalysts specifically designed to address the critical issue of water pollution. Zinc oxide (ZnO) remains a material of significant interest in this field due to its wide bandgap of approximately 3.37 eV, which allows for effective charge separation and enhanced photocatalytic activity. Its advantageous properties facilitate both energy conversion processes and environmental remediation efforts. However, it is important to note that ZnO's solar absorption capabilities are primarily confined to the ultraviolet spectrum (wavelengths below 400 nm), which poses challenges for its application under visible light conditions. This study explores various modifications and enhancements to ZnO, aiming to broaden its absorption spectrum and improve its photocatalytic efficiency in degrading pollutants in water systems. By leveraging advanced synthesis techniques and composite material approaches, this research seeks to optimize the performance of ZnO-based photocatalysts, ultimately contributing to cleaner water solutions [19].

2. Synthesis Materials

Commercial zinc oxide powder, ethyl alcohol, deionized water, sodium hydroxide (NaOH) ammonium tetrathiomolybdate [$(NH_4)_2MoS_4$], hydrazine (N_2H_4), Methylene Blue (MB), $Na_2MoO_4.2H_2O$, Zn $(CH_3COO)_2.2H_2O$, CS $(NH_2)_2$ etc.

2.1 Synthesis of ZnO Nanorods

In this synthesis process, 0.015 moles of commercial ZnO powder were carefully dissolved in 10 mL of a concentrated 10 mol/L NaOH solution. To this mixture, 490 mL of water was added, creating a homogenous solution. The resulting mixture was subjected to microwave irradiation, where it was heated to a precise temperature of 600°C for 20 minutes. Following this heating phase, the solution was allowed to cool, and a white precipitate formed, which was subsequently collected through filtration. The precipitate was thoroughly washed sequentially with distilled water and ethanol to ensure purity, resulting in a refined final product [6, 10].

2.2 Synthesis of MoS_2 nanosheets

In this experimental procedure, 0.05 grams of ammonium tetrathiomolybdate [$(NH4)_2MoS_4$] powder was carefully dispersed in a well-stirred mixture of 10 ml of ethanol and 10 ml of distilled water, maintaining a constant stirring for one hour to ensure uniform distribution. Following this, 1 ml of hydrazine hydrate (N_2H_4) was gradually introduced into the solution, initiating a chemical reaction. To enhance the dispersion of the materials, the mixture was subjected to sonication for an impressive duration of 10 hours in an ultrasonic bath, which helped to break down the aggregates and produce fine MoS_2 sheets. After sonication, the resultant dispersion was centrifuged at 3000 rpm for 10 minutes to facilitate the purification of the MoS_2 sheets [20–22]. The purified product was then carefully dispersed in 30 ml of ethanol, preparing it for subsequent characterization.

2.3 Synthesis of MoS_2 / ZnO hybrid structures

A specific quantity of molybdenum disulfide was meticulously incorporated into a 300 mL suspension of ethanol, which included 0.5 g of zinc oxide (ZnO) nanosheets. This mixture was subjected to continuous stirring for 24 hours to ensure thorough dispersion and interaction between the components. Afterward, the combined solution underwent centrifugation at a speed of 2000 rpm to separate the solid particles from the liquid phase. The resulting precipitate was subsequently washed multiple times with ethanol to remove any unreacted materials and impurities. The final product was then dried overnight in an oven at a temperature of 250°C to eliminate residual solvent and consolidate the heterojunction structure. This naming convention reflects the precise ratio of MoS_2 incorporated within the ZnO matrix, which is expected to influence the heterojunction's properties and potential applications in various fields, such as photocatalysis, optoelectronics, and energy storage.

3. Results and Discussion

3.1 XRD analysis of ZnO-MoS_2 hybrid structures

The X-ray diffraction (XRD) patterns of all prepared powder samples were meticulously recorded over a comprehensive range of diffraction angles from 10° to 80° at room temperature. The XRD pattern of molybdenum disulfide (MoS_2) reveals distinct peaks at 14.4°, 33.1°, and 58.5°, corresponding to the lattice planes (002), (103), and (105), respectively (**Figure 1).** These sharp peaks confirm the successful synthesis of two-dimensional (2D) pure phase MoS_2, indicating a well-ordered crystalline structure and high quality of the material. In parallel, the XRD patterns of zinc oxide (ZnO) exhibit prominent peaks that are characteristic of wurtzite nanostructures, with notable diffraction peaks observed at 31.8°, 34.4°, and 36.2°. These features not only demonstrate the crystalline integrity of the ZnO but also confirm the successful formation of the desired structure. Importantly, the XRD patterns of the synthesized ZnO-MoS_2 hybrid structure exhibited no extra peaks, which suggests that the composite material maintains phase purity and homogeneity. The absence of unexpected peaks indicates that there are no unwanted phases or impurities present, thereby reinforcing the structural integrity of the hybrid structures. This highlights the effectiveness of the synthesis method used and the compatibility of the individual components at the nanoscale level [12].

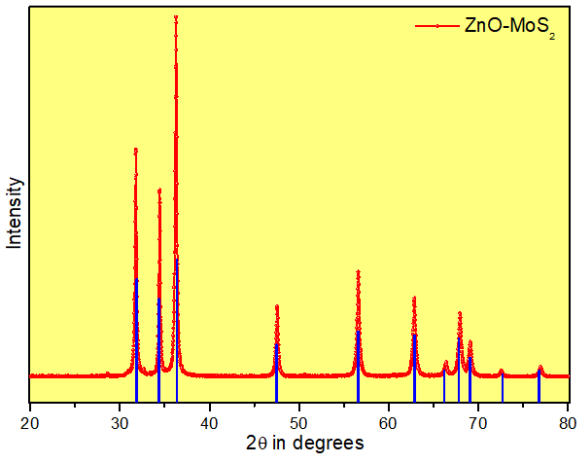

Figure 1: X-ray diffraction pattern of synthesized ZnO-MoS_2 hybrid structure

3.2 UV Vis spectra analysis of ZnO-MoS_2 hybrid structures

The UV-vis spectra of MoS_2 nanoflakes and the ZnO-MoS_2 hybrid structure are illustrated in **Figure 2**, spanning the wavelength range of 300 to 700 nm. Notably, the MoS_2/ZnO hybrid structures exhibited significantly enhanced light absorption compared to the individual components. This result underscores the impact of integrating ZnO with MoS_2 into the ZnO-MoS_2 hybrid structures, markedly improving its light-harvesting capabilities. Pure ZnO, characterized by an absorption edge around 365 nm, demonstrated substantial absorption primarily within the ultraviolet (UV) region, indicating its potential for UV-driven applications. In contrast, the ZnO-MoS_2 hybrid structure, which displayed distinctive orange hues, exhibited significantly greater absorption in the visible light spectrum when compared to the weak blue absorption of pure ZnO.

This enhanced absorption in the visible region can be attributed to the introduction of MoS_2, which facilitates a broader light absorption profile. Moreover, the incorporation of MoS_2 nanoparticles into the ZnO matrix enabled the hybrid structures to absorb light effectively across the entire UV/Vis range (300-700 nm). This comprehensive absorption spectrum not only improves the photocatalytic properties of the material but also highlights the synergistic interactions between MoS_2 and ZnO, making ZnO-MoS_2 hybrid structure promising candidates for various optoelectronic and photocatalytic applications [11, 23].

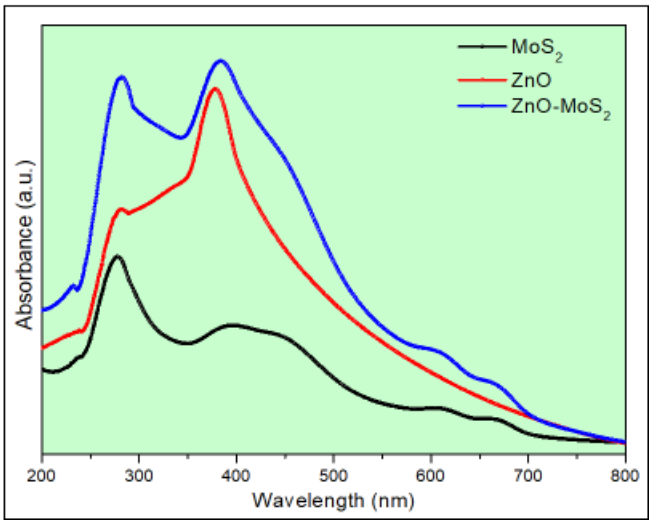

Figure 2: UV – V is spectra of MoS_2 nanoflakes and ZnO-MoS_2 hybrid structure

3.3 TEM analysis of ZnO-MoS_2 hybrid structures

We conducted a detailed investigation into the microstructure of the synthesized samples. The vertically aligned zinc oxide (ZnO) nanorods (NRs) are illustrated in **Figure 3 (a-d),** which include selected area electron diffraction (SAED) and transmission electron microscopy (TEM) images, respectively. Our analysis revealed that the average side-to-side diameter of the hexagonal nanorods is approximately 124.7 nanometers.

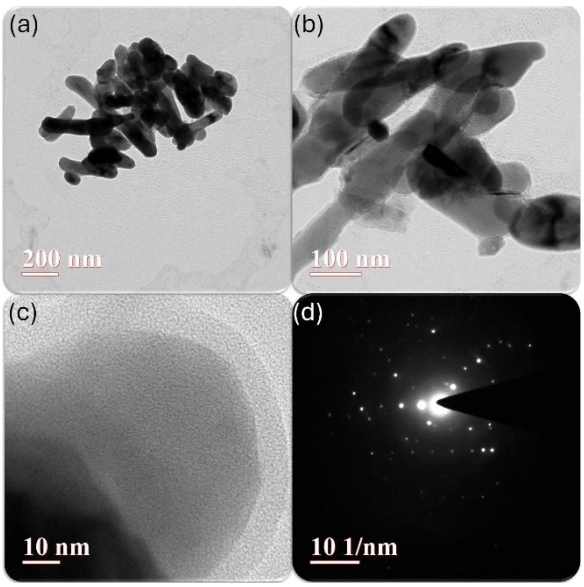

Figure 3: (a-b) TEM (c) HRTEM and (d) SAED image of ZnO-MoS_2 hybrid structure

Utilizing the X-ray diffraction (XRD) data presented previously in the figures, we identified an interplanar spacing of 0.26 nanometers from high-resolution TEM imagery, which can be attributed to the (002) plane of ZnO. However, further analysis depicted that these nanoparticles (NPs) are likely composed of zinc sulfide (ZnS) coated with multiple layers of molybdenum disulfide (MoS_2) nanosheets. Previous literature indicates that under optimal conditions, specifically regarding the concentration of the sulfur precursor and the duration of the reaction, the outer layer of ZnO NRs can undergo a transformation to ZnS. Despite

several ZnO NRs maintaining their characteristic hexagonal rod shape, we can observe signs of partial conversion from ZnO to ZnS. In our experimental setup, the transformation is driven by the interaction of sulfur derived from CH_3CSNH_2 with the ZnO NRs. Moreover, there is additional sulfur present that interacts with sodium molybdate dihydrate ($Na_2MoO_4 \cdot 2H_2O$), facilitating the formation of low-density MoS_2 nanosheets [20, 24, 25]. To create zinc sulfide-molybdenum disulfide (ZSM) hybrid structures, these few-layer MoS_2 nanosheets aggregate and envelop the outer layers of the ZnO/ZnS composite. The high-resolution TEM images provide compelling evidence of the three distinct phases—ZnO, ZnS, and MoS_2—by displaying three separate lattice fringes. Specifically, the interlayer spacing of 0.69 nanometers is consistent with the (002) plane of MoS_2, while interlayer spacings of 0.32 nanometers and 0.26 nanometers correspond to the (111) facets of ZnS and the (002) plane of ZnO, respectively. These measurements correlate well with our findings from the crystallographic analysis, further confirming the structural integrity and morphological attributes of the synthesized nanostructures.

3.4 FTIR analysis of ZnO-MoS_2 hybrid structures

To investigate the presence of functional groups and metallic bonds, Fourier Transform Infrared (FTIR) spectroscopy analyses were conducted over a wavenumber range of 400 to 4000 cm^{-1} at ambient temperature. The FTIR spectra for zinc oxide (ZnO), molybdenum disulfide (MoS_2), and the composite MoS_2-ZnO are presented in **Figure 4**. The results confirm the formation of metal-oxygen bonds within both ZnO and MoS_2. Prominent peaks at approximately 497 cm^{-1} and 700 cm^{-1} correspond to the Zn-O bond and the Mo-S bond, respectively.

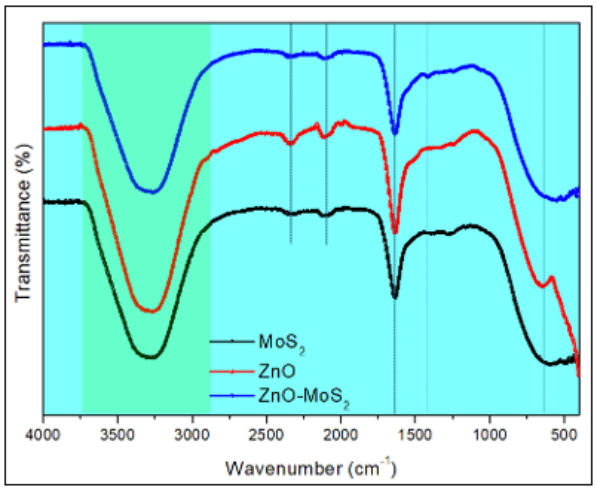

Figure 4: FTIR spectra of ZnO, MoS_2, and ZnO-MoS_2 hybrid structure

Additionally, a broad peak near 1000 cm^{-1} indicates the presence of hydrogen-oxygen bonds, likely sourced from the ambient moisture. For ZnO, strong absorption bands are observed at approximately 3400 cm^{-1}, 1550 cm^{-1}, and 463.36 cm^{-1}, which are attributed to O–H stretching, H–O–H bending vibrations, and Zn–O stretching vibrations, respectively [26, 27]. In the case of MoS_2, a distinct peak at around 935 cm^{-1} is attributed to S-S bond vibrations, while a peak at approximately 469 cm^{-1} corresponds to Mo-S stretching vibrations. Notably, both ZnO and MoS_2 exhibit a significant absorption band near 3440 cm^{-1}, which is linked to O–H and H–O–H stretching vibrations, further highlighting interactions with moisture. This comprehensive spectral analysis underscores the distinct bonding characteristics and the potential interactions occurring within the materials under investigation.

3.5 XPS analysis of ZnO-MoS_2 hybrid structures

In X-ray Photoelectron Spectroscopy (XPS), the analysis revealed the presence of multiple components acting as photocatalysts within the sample. According to the literature, **Figure 5 (a-d)** illustrates the comprehensive survey of ZnO alongside high-resolution scans of the Mo3d, Zn2p, and S2p peaks, along with their optimal deconvolution into individual components. Notably, in the MoS_2 3d spectra, two distinct peaks corresponding to the Mo 3d3/2 and Mo 3d5/2 states were identified at 229.2 eV and 232.8 eV, respectively [28]. These energy levels confirm the oxidation states of molybdenum within the MoS_2 structure. Furthermore, because the MoS_2 lattice does not alter the chemical makeup of the ZnO nanoparticles, the two peaks observed in the O1s spectra at 532.6 eV and 531.3 eV can be attributed, respectively, to the oxygen functionalities associated with the organic linkers in the structure and the ZnO lattice oxygens bonded to the ZnO nanoparticles.

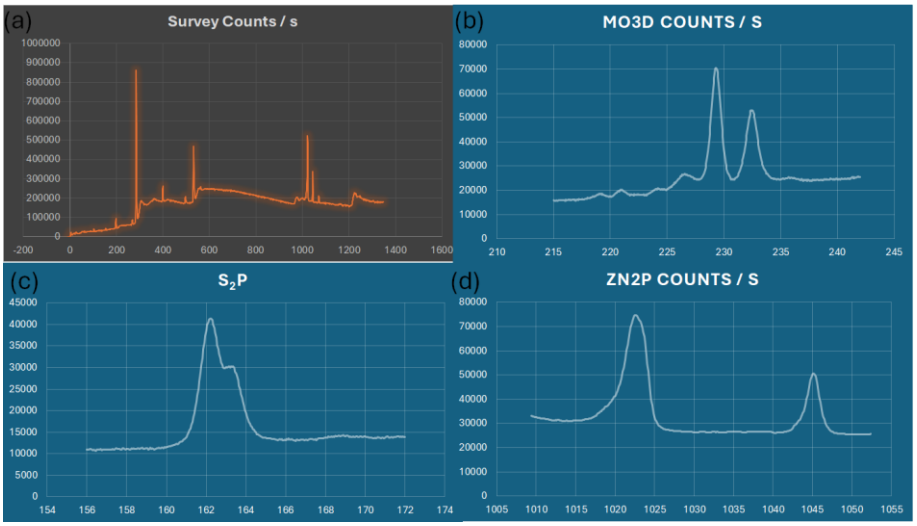

Figure 5: XPS Analysis of MoS_2 nanoflakes and MoS_2/ZnO hybrid structures (a) Survey (b) MoS_2 (c) S2p and (d) ZnO NPs

Additionally, the presence of nitrogen (N) and sulfur (S) dopants on the surface of the MoS_2 was conclusively demonstrated through the XPS analysis. The high-resolution N1s spectrum reveals a peak at 401.1 eV, distinctly indicating the presence of MoS_2-N bonds, which suggests the incorporation of nitrogen into the MoS_2 framework. Moreover, in the high-resolution S2p spectrum, a prominent single peak at a binding energy of 163.4 eV was observed. This peak is attributed to carbon-sulfur (CS) bonding, further supporting the presence of sulfur functionalities incorporated within the MoS_2 matrix, as deduced from the extensive characterization data acquired during the study. This comprehensive analysis establishes a clearer understanding of the electronic environment and bonding characteristics within the investigational materials [12, 17, 29].

3.6 Photocatalytic Analysis of ZnO-MoS_2 Hybrid Structures

To effectively degrade the dye, a ZnO-MoS_2 hybrid structure was employed as a photocatalytic semiconductor in the presence of a light source. The analysis of the absorbance versus wavelength graph indicates that the degradation efficiency of the ZnO-MoS_2 hybrid structures surpasses that of individual ZnO and MoS_2 components. Specifically, the ZnO-MoS_2 hybrid structure achieved an impressive dye degradation rate of up to 90% within just 45 minutes, as illustrated in the corresponding graph. In this study, we utilized as-synthesized MoS_2, ZnO, and ZnO-MoS_2 hybrid structures as photocatalysts for the degradation of Methylene Blue (MB). **Figure 6 (a)** presents the UV-Vis absorption spectra used to investigate the photocatalytic degradation of a 5 µM MB solution [30, 31]. These samples were irradiated with direct solar energy for a duration of 45 minutes, allowing us to monitor the degradation process effectively. The characteristic absorption peak for MB was observed at 660 nm, and this peak intensity was tracked as a function of exposure time to solar energy. The kinetics of the photocatalytic degradation of MB dyes with the ZnO and ZnO-MoS_2 hybrid structure conform to first-order kinetics, as demonstrated in **Figure 6 (b).** The results show that the as-prepared ZnO and ZnO-MoS_2 hybrid structures facilitated photocatalytic degradation of 41% and 81% of the 5 µM MB solution, respectively, as illustrated in **Figure 6 (c).** The calculated rate constants for the degradation processes were determined to be 29.1 × 10^{-3} min^{-1} for ZnO and 74.1 × 10^{-3} min^{-1} for the ZnO-MoS_2 hybrid structure. Additionally, we evaluated the recyclability and eco-friendly characteristics of both ZnO and ZnO-MoS_2 photocatalysts by performing multiple degradation cycles with the same samples, repeating the reactions for three consecutive cycles, as presented in **Figure 6 (d).** The synthesized ZnO-MoS_2 hybrid structures show great potential for practical photocatalytic applications, demonstrating not only high efficiency but also sustainability in environmental remediation efforts [32, 33].

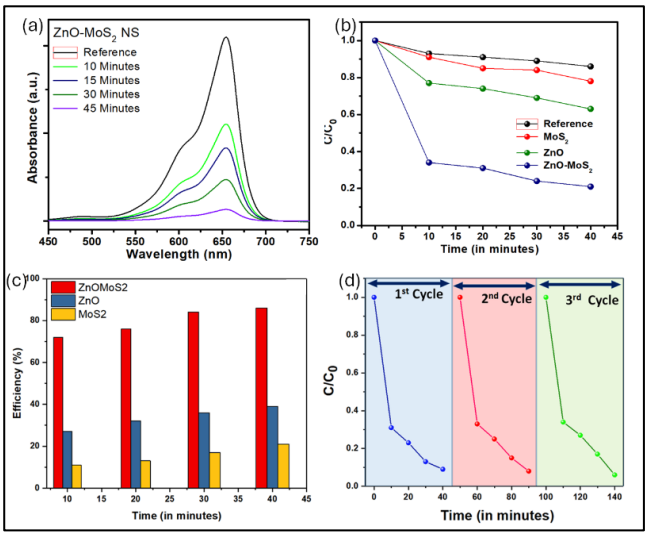

Figure 6: (a) UV-Vis absorption spectra for photocatalytic degradation of 5 µM for the degradation of Methylene Blue (MB) for the synthesized materials (b) Rate Constant (c) Efficiency and (d) Reusability of ZnO-MoS_2 hybrid structures

4. Conclusion

The ZnO-MoS_2 hybrid structures have been successfully synthesized, marking a significant advancement in composite material development. The X-ray diffraction (XRD) pattern distinctly confirmed the crystal structure and average particle size of the composite, indicating a well-defined arrangement at the atomic level. Furthermore, the UV-visible spectroscopy of MoS_2 sheets and the ZnO-MoS_2

hybrid structure illustrated a broad absorption capacity spanning the entire ultraviolet to visible spectrum (300-700 nm), showcasing their potential for light-harvesting applications. The Raman spectrum of the ZnO-MoS_2 hybrid structure revealed the presence of pure phases of both MoS_2 and ZnO, effectively validating the findings from the XRD analysis. High-resolution transmission electron microscopy (TEM) images portrayed the nanoparticles as being well within the nanoscale range, characterized by a uniform formation of hexagonal nanorods. Remarkably, the average diameter across the hexagonal nanorods measured 124.7 nm, emphasizing their consistent architectural design. The polycrystalline nature of the ZnO-MoS_2 hybrid structure was further corroborated through high-resolution TEM imaging, which revealed an interplanar distance between the fringes measuring 0.26 nm, indicative of high-quality crystallinity. To assess the practical application of these hybrid structures, their feasibility as photocatalysts was rigorously tested. The degradation efficiency of the ZnO-MoS_2 hybrid structure exceeded that of both ZnO and MoS_2 alone, attributed to the enhanced specific surface area of the photocatalyst and improved separation efficiency of photogenerated electron-hole pairs resulting from the MoS_2 layer coating on the ZnO nanorods. Impressively, the ZnO-MoS_2 hybrid structure achieved a dye degradation rate of up to 90% for methylene blue (MB) within just 45 minutes, highlighting the extraordinary photocatalytic degradation activity of the ZnO-MoS_2 hybrid structure. These findings suggest that the integration of MoS_2 with ZnO significantly enhances the efficacy of photocatalytic processes, paving the way for advanced applications in environmental remediation and beyond.

Credit authorship contribution agreement

Priyavrat: Methodology, Investigation, Visualization, Writing-original draft, Writing-review & editing, **Ariba Khan:** Methodology, Investigation, Writing-original draft, Writing-review & editing. **Anil Kumar Singh** and **Jamilur R. Ansari:** Supervision, Validation, Project administration, funding acquisition, writing-review & editing. All the authors have read and discussed the data and agreed to the published version of the manuscript.

Conflicts of Interest

The authors declare that they have no conflict of interest.

Acknowledgments

Priyavrat gratefully acknowledges the support from VKSU, Ara, in the form of a Research Fellowship. **Ariba Khan** is thankful to the Director of LIET, Alwar, for the support. The authors thank Yonsei University for carrying out TEM/HRTEM characterizations. **Jamilur R. Ansari** is thankful to LIET, Alwar, and Yonsei University for the support under the BP Program, and **Anil Kumar Singh** is thankful to VKSU, Ara, for the support.

References

[1] M. Vasylius, A. Tadžijevas, D. Šapalas, V. Kartašovas, J. Janutėnienė, P. Mažeika, Degradation of Mechanical Properties of A-PET Films after UV Aging, Polymers 15 (2023) 4166. https: //doi. org/10.3390/polym15204166.

[2] Y. Xu, Z. Wu, A. Li, N. Chen, J. Rao, Q. Zeng, Nanocellulose Composite Films in Food Packaging Materials: A Review, Polymers 16 (2024) 423. https: //doi. org/10.3390/polym16030423.

[3] S. Kapoor, V. Kumar, K. B. Tikoo, B. Chudasama, N. Goel, S. Singhal, Strategically designed reduced graphene oxide based magnetic responsive nanocatalysts for the attenuation of recalcitrant pollutants, Ceram. Int.46 (2020) 2724–2742. https: //doi. org/10.1016/j. ceramint.2019.09.262.

[4] W. J. Chong, S. Shen, Y. Li, A. Trinchi, D. Pejak, I. (Louis) Kyratzis, A. Sola, C. Wen, Additive manufacturing of antibacterial PLA-ZnO nanocomposites: Benefits, limitations and open challenges, J. Mater. Sci. Technol.111 (2022) 120–151. https: //doi. org/10.1016/j. jmst.2021.09.039.

[5] S. Roy, H. C. Kim, P. S. Panicker, J.-W. Rhim, J. Kim, Cellulose Nanofiber-Based Nanocomposite Films Reinforced with Zinc Oxide Nanorods and Grapefruit Seed Extract, Nanomaterials 11 (2021) 877. https: //doi. org/10.3390/nano11040877.

[6] F. T. Thema, E. Manikandan, M. S. Dhlamini, M. Maaza, Green synthesis of ZnO nanoparticles via Agathosma betulina natural extract, Mater. Lett.161 (2015) 124–127. https: //doi. org/10.1016/j. matlet.2015.08.052.

[7] J. R. Ansari, N. Singh, S. Anwar, S. Mohapatra, A. Datta, Silver nanoparticles decorated two dimensional MoS2 nanosheets for enhanced photocatalytic activity, Colloids Surf. Physicochem. Eng. Asp.635 (2022) 128102. https: //doi. org/10.1016/j. colsurfa.2021.128102.

[8] X. Gan, H. Zhao, X. Quan, Two-dimensional MoS2: A promising building block for biosensors, Biosens. Bioelectron.89 (2017) 56–71. https: //doi. org/10.1016/j. bios.2016.03.042.

[9] S. Thakur, P. Bandyopadhyay, S. H. Kim, N. H. Kim, J. H. Lee, Enhanced physical properties of two dimensional MoS2/poly (vinyl alcohol) nanocomposites, Compos. Part Appl. Sci. Manuf.110 (2018) 284–293. https: //doi. org/10.1016/j. compositesa.2018.05.009.

[10] F. Wang, M. Cao, Y. Qin, J. Zhu, L. Wang, Y. Tang, ZnO nanoparticle-decorated two-dimensional titanium carbide with enhanced supercapacitive performance, RSC Adv.6 (2016) 88934–88942. https: //doi. org/10.1039/C6RA15384D.

[11] S. R. Gottam, C.-T. Tsai, C.-Y. Li, S.-Y. Chu, Investigation of MoS_2 Nanosheet-Coated ZnO Thin Films for Hydrogen Gas Sensing Applications and the Effect of Temperature on the Enhanced Sensor Response, J. Electrochem. Soc.167 (2020) 087507. https: //doi. org/10.1149/1945-7111/ab8f59.

[12] T. Yang, M. Chen, Q. Kong, X. Luo, K. Jiao, Toward DNA electrochemical sensing by free-standing ZnO nanosheets grown on 2D thin-layered MoS2, Biosens. Bioelectron.89 (2017) 538–544. https: //doi. org/10.1016/j. bios.2016.03.025.

[13] O. Samy, S. Zeng, M. D. Birowosuto, A. El Moutaouakil, A Review on MoS2 Properties,

Synthesis, Sensing Applications and Challenges, Crystals 11 (2021) 355. https: //doi. org/10.3390/cryst11040355.
[14] Q. Liang, L. Jiang, J. Zheng, N. Duan, Determination of High Concentration Copper Ions Based on Ultraviolet—Visible Spectroscopy Combined with Partial Least Squares Regression Analysis, Processes 12 (2024) 1408. https: //doi. org/10.3390/pr12071408.
[15] N. Ben Halima, Poly (vinyl alcohol): review of its promising applications and insights into biodegradation, RSC Adv.6 (2016) 39823–39832. https: //doi. org/10.1039/C6RA05742J.
[16] H. S. Nalwa, A review of molybdenum disulfide (MoS $_2$) based photodetectors: from ultra-broadband, self-powered to flexible devices, RSC Adv.10 (2020) 30529–30602. https: //doi. org/10.1039/D0RA03183F.
[17] J. Kabel, S. Sharma, A. Acharya, D. Zhang, Y. K. Yap, Molybdenum Disulfide Quantum Dots: Properties, Synthesis, and Applications, C 7 (2021) 45. https: //doi. org/10.3390/c7020045.
[18] J. Ma, Y. Li, X. Yin, Y. Xu, J. Yue, J. Bao, T. Zhou, Poly (vinyl alcohol) /graphene oxide nanocomposites prepared by in situ polymerization with enhanced mechanical properties and water vapor barrier properties, RSC Adv.6 (2016) 49448–49458. https: //doi. org/10.1039/C6RA08760D.
[19] C. Wu, K. Liu, Y. Li, L. Wang, S. Guo, Y. Sun, F. Zhang, G. Shao, P. Zhang, Dual-Modified Hollow Spherical Shell MoS $_2$[at]TiO $_2$ /TiN Composites for Photocatalytic Hydrogen Production, Energy Technol.10 (2022) 2100265. https: //doi. org/10.1002/ente.202100265.
[20] M. Donarelli, L. Ottaviano, 2D Materials for Gas Sensing Applications: A Review on Graphene Oxide, MoS2, WS2 and Phosphorene, Sensors 18 (2018) 3638. https: //doi. org/10.3390/s18113638.
[21] O. Samy, S. Zeng, M. D. Birowosuto, A. El Moutaouakil, A Review on MoS2 Properties, Synthesis, Sensing Applications and Challenges, Crystals 11 (2021) 355. https: //doi. org/10.3390/cryst11040355.
[22] Y. Wang, F. Chen, X. Ye, T. Wu, K. Wu, C. Li, Photoelectrochemical immunosensing of tetrabromobisphenol A based on the enhanced effect of dodecahedral gold nanocrystals/MoS2 nanosheets, Sens. Actuators B Chem.245 (2017) 205–212. https: //doi. org/10.1016/j. snb.2017.01.140.
[23] S. Roy, R. Priyadarshi, J.-W. Rhim, Development of Multifunctional Pullulan/Chitosan-Based Composite Films Reinforced with ZnO Nanoparticles and Propolis for Meat Packaging Applications, Foods 10 (2021) 2789. https: //doi. org/10.3390/foods10112789.
[24] P. Berwal, S. Rani, S. Sihag, P. Singh, R. Dahiya, A. Kumar, A. Sanger, A. K. Mishra, V. Kumar, Hydrothermal synthesis of MoS2 with tunable band gap for future nano-electronic devices, Inorg. Chem. Commun.159 (2024) 111833. https: //doi. org/10.1016/j. inoche.2023.111833.
[25] F. Chekin, R. Boukherroub, S. Szunerits, MoS2/reduced graphene oxide nanocomposite for sensitive sensing of cysteamine in presence of uric acid in human plasma, Mater. Sci. Eng. C 73 (2017) 627–632. https: //doi. org/10.1016/j. msec.2016.12.102.
[26] H. Sun, J. Chao, X. Zuo, S. Su, X. Liu, L. Yuwen, C. Fan, L. Wang, Gold nanoparticle-decorated MoS2 nanosheets for simultaneous detection of ascorbic acid, dopamine and uric acid, RSC Adv.4 (2014) 27625. https: //doi. org/10.1039/c4ra04046e.
[27] A. Sinha, Dhanjai, B. Tan, Y. Huang, H. Zhao, X. Dang, J. Chen, R. Jain, MoS2 nanostructures for electrochemical sensing of multidisciplinary targets: A review, TrAC Trends Anal. Chem.102 (2018) 75–90. https: //doi. org/10.1016/j. trac.2018.01.008.
[28] M. C. Biesinger, B. P. Payne, A. P. Grosvenor, L. W. M. Lau, A. R. Gerson, R. St. C. Smart, Resolving surface chemical states in XPS analysis of first row transition metals, oxides and hydroxides: Cr, Mn, Fe, Co and Ni, Appl. Surf. Sci.257 (2011) 2717–2730. https: //doi. org/10.1016/j. apsusc.2010.10.051.
[29] M. Choi, J. Lim, J. Yang, Synergistic role of MoS2 in gelation-induced fabrication of graphene oxide films, Sci. Rep.14 (2024) 12159. https: //doi. org/10.1038/s41598-024-62146-4.
[30] G. Deme, A. Belay, D. M. Andoshe, G. Barsisa, D. Tsegaye, S. Tiruneh, C. Seboka, Effect of Hydrothermal Reaction Temperature on Fluorescent Properties of Carbon Quantum Dots Synthesized from Lemon Juice for Adsorption Applications, J. Nanomater.2023 (2023) 1–10. https: //doi. org/10.1155/2023/1701496.
[31] N. U. M. Nizam, M. M. Hanafiah, E. Mahmoudi, A. W. Mohammad, Synthesis of highly fluorescent carbon quantum dots from rubber seed shells for the adsorption and photocatalytic degradation of dyes, Sci. Rep.13 (2023) 12777. https: //doi. org/10.1038/s41598-023-40069-w.
[32] S. Bhandari, D. Mondal, S. K. Nataraj, R. G. Balakrishna, Biomolecule-derived quantum dots for sustainable optoelectronics, Nanoscale Adv.1 (2019) 913–936. https: //doi. org/10.1039/C8NA00332G.
[33] R. Wang, K.-Q. Lu, Z.-R. Tang, Y.-J. Xu, Recent progress in carbon quantum dots: synthesis, properties and applications in photocatalysis, J. Mater. Chem. A 5 (2017) 3717–3734. https: //doi. org/10.1039/C6TA08660H.